

High energy and high power primary Li-CF_x batteries enabled by the combined effects of the binder and the electrolyte

Haobin Huo¹, Leon L. Shaw¹ and Károly Németh^{2,*}

¹ Mechanical, Materials, and Aerospace Engineering Department; hhuo2@hawk.iit.edu, lshaw2@iit.edu

² Physics Department, Illinois Institute of Technology; knemeth@iit.edu

* Correspondence: knemeth@iit.edu

Abstract: Several effective methods have been developed recently to demonstrate simultaneous high energy and high power density in Li - carbon fluoride (CF_x) batteries. These methods can achieve as high as 1000 Wh/kg energy density at 60-70 kW/kg power density (40-50 C rate) in coin cells and 750 Wh/kg energy density at 12.5 kW/kg power density (20 C rate) in pouch cells. This performance is made possible by ingenious nano-architecture design, controlled porosity, boron doping and electrolyte additives. In the present study, we show that a similarly great performance, 931 Wh/kg energy density at 59 kW/kg power density, can be achieved by using a polyacrylonitrile binder and a LiBF₄ electrolyte in Li - graphite fluoride coin cells. We also demonstrate that the observed effect is the result of the right combination of the binder and the electrolyte. We propose that the mechanistic origin of the observed phenomena is an electro-catalytic effect by the polyacrylonitrile binder. While our proposed method has a competitive performance, it also offers a simple implementation and a scalable production of high energy and high power primary Li-CF_x cells.

Keywords: graphite fluoride; battery; polyacrylonitrile; lithium fluoride, crystal growth, inhibition, amorphization

1. Introduction

Functionalized two-dimensional (2D) materials as cathode active species have a demonstrated ability to realize simultaneously high energy and high power in primary and secondary batteries. These features are highly desirable for many applications ranging from electric cars to electric aircraft, space exploration, pulsed power sources and medical devices [1–7]. Graphite fluoride (CF_x, 0 < x < 1.3) is the oldest known example of functionalized 2D materials as cathode active species. The structure of fully fluorinated graphite is known since 1947 and consists of stacked fluorinated layers of graphene [8,9]. The Li-CF_x primary battery was commercialized in 1970 [10–12]. It offers many advantages such as high energy and high power density, excellent shelf life, applicability in a wide temperature range (–60 to +60 °C) and a relatively easy to source and economic composition [13–17]. It has a very high theoretical specific energy of 2180 Wh/kg at a capacity of 864 mAh/g when graphite is fully fluorinated (x ≈ 1) and an open circuit voltage (OCV) of 3.2-3.3 V [10]. It is a primary battery with only a limited degree of rechargeability [18,19]. The cell reaction on discharge is the following:



If the discharge product carbon would be graphite, an OCV of 4.57 V should be observed on the basis of thermodynamical calculations [20,21]. The much lower observed OCV is a consequence of the formation of a sandwich structure of LiF and graphene in the discharge product [20–22].

The study of solvent effects led to the recognition that the solvated Li⁺ ion intercalates between the stacked CF_x monolayers during discharge and the solid LiF discharge product forms only after the collapse of the solvent shell of Li⁺ between the CF_x layers [21,22]. The higher the solvation energy of Li⁺ in a given solvent the lower the discharge voltage [22].

The intercalation of solvated Li⁺ ions was also seen in graphene oxide (GO) cathodes. In order to achieve high power density in Li/Na-GO batteries, the GO interlayer distance must be expanded, which is typically achieved via a thermal treatment of GO before building the cathode [23–27]. The layer distance in fully fluorinated CF_x is about 6-9 Å [9] and the interaction between the layers is weak enough to allow for the penetration of some solvated Li⁺ ions.

The discharged CF_x (which includes the intercalated CF_x and its discharge products) typically forms a shell around a core of CF_x particles and has a major impact on the overall performance of the Li- CF_x cells [28]. The time evolution of the structure and composition of the cathode during discharge has been studied recently in detail at a slow discharge rate [29]. As opposed to expectations, the graphene layers transform into a hard carbon structure during discharge with a much reduced sp^2 carbon content. The optimization of the structure and composition of the domain of the discharged CF_x is the key to improving the electrochemical performance of Li- CF_x cells.

The specific power of Li- CF_x cells used to be small historically. In 2007, commercial Li- CF_x batteries were reported to have a break-down of specific energy at a specific power of ≈ 1.6 kW/kg which was cured by the introduction of partially fluorinated CF_x ($\approx 0.3 < x < \approx 0.8$) cathodes. Partially fluorinated CF_x could realize much higher specific power values and a break-down of specific energy at 10 kW/kg [30,31]. Research on high power Li- CF_x batteries intensified in the past decade. Various approaches have been developed which are capable to deliver a specific energy of 800-1000 Wh/kg at power densities of 20-70 kW/kg (15-50 C rates). These approaches utilize nano-architecture design, such as fluorinated graphene microspheres [32], increased porosity and edge (instead of in-plane) functionalization [33–36] and amorphization of the discharge product LiF [37]. Recently, the amorphization of LiF was achieved by the addition of BF_3 gas in the electrolyte at a 0.01 M concentration and was confirmed by the lack of LiF pattern in the X-ray diffraction pattern of the discharged CF_x cathode [37]. Amorphization of LiF was also observed when a solid electrolyte, Li_3PS_4 was used [38].

Another method of amorphization of the discharge product LiF was proposed by Jones and Hossain about a decade ago as a way to reduce the relatively high heat production during discharge [39]. These inventors proposed to use polymeric binders that serve a dual purpose: (1) they mechanically bind components of the cathode together and (2) act as complexation / amorphization agents of LiF. Several such polymers were proposed as a replacement of the more traditional poly(vinylidene difluoride) (PVDF) and teflon (PTFE), among them polyacrylonitrile (PAN) derivatives (primarily complexing the Li^+ ions) and boronates (primarily complexing F^- ions). These complexation phenomena are typically based on Lewis acid-base reactions. The gaseous BF_3 electrolyte additive mentioned above is a simple example of the formation of a Lewis adduct of LiF with BF_3 as BF_3 is well known to easily dissolve LiF in the form of LiBF_4 . Unfortunately, the theoretical proposal of Jones and Hossain has not been experimentally demonstrated to date, to the best of our knowledge.

We have been working on the development of high energy and high power batteries based on functionalized 2D materials for about a decade [40–45]. We recently proposed the use of adducts of BF_3 with graphene oxide (GO) and oxidized hexagonal boron nitride (hBN) as cathode active species and solid electrolytes [42–45].

The above mentioned successful application of the BF_3 gas additive in Li- CF_x cells [37] has called our attention to the role of BF_3 and its adducts in high power Li- CF_x cells. However, our initial attempt to use BF_3 -etherate as a safer alternative to BF_3 gas in Li- CF_x cells to achieve high power density has failed. This has motivated us to investigate alternatives. We have explored the use of $\text{LiOX} \cdot \text{BF}_3$ ($X = \text{Li}, \text{H}$) to substitute -F to - OBF_3 groups in CF_x for a greater interlayer spacing. As the addition of $\text{LiOX} \cdot \text{BF}_3$ led to an alkaline cathode, we have thus also investigated a PAN binder instead of the traditional PVDF because the latter is not stable in alkaline environment [46]. This study has resulted in the discovery of the beneficial effects of a PAN binder on the power density of Li- CF_x cells. Furthermore, we have discovered that such a binder effect occurs only in selected electrolytes. While the mechanistic origin of the combined binder and electrolyte effects are not clear yet, we propose that it is likely related to the electro-catalytic activity of PAN. The details of our findings are described below.

2. Materials and Methods

Graphite fluoride (CF_x) was purchased from ACS Material (product number GT1FS012) with the F/C ratio being 0.8-1.1. The X-ray diffraction (XRD) pattern (at Cu $K\alpha$ X-ray radiation) of this CF_x is shown in Fig 1. The (002) reflection at 26.7 deg indicates the presence of some unfluorinated graphite species.

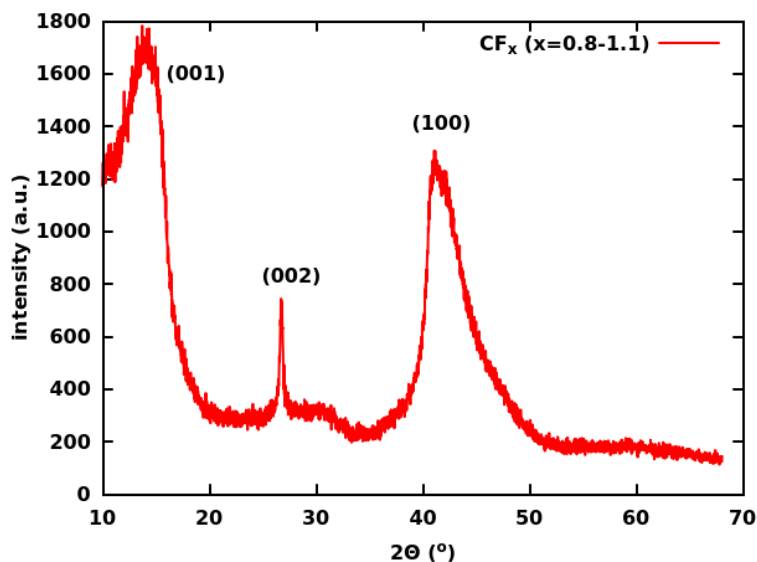


Figure 1. XRD (Cu $K\alpha$) pattern of the CF_x used in the present study. The presence of some unfluorinated graphite is indicated by the (002) reflection.

Lithium tetrafluoroborate ($LiBF_4$), lithium perchlorate ($LiClO_4$), lithium hexafluorophosphate ($LiPF_6$), lithium bis(oxalato)borate ($LiB(C_2O_4)_2$, LiBOB), polyacrylonitrile (PAN, average molecular weight 150000), carbon black (CB), ethylene carbonate (EC), dimethyl carbonate (DMC), propylene carbonate (PC), 1,2 dimethoxy ethane (DME), dimethyl sulfoxide (DMSO), 1,3-dioxalane (DOL), N,N-dimethylformamide (DMF) and N-Methyl-2-pyrrolidone (NMP) were purchased from Millipore-Sigma. Poly(vinylidene difluoride) (PVDF) was purchased from Alfa Aesar. Conductive carbon black (CB, TIMCAL Graphite & Carbon Super P) was purchased from MTI Corporation. The as purchased LiBOB was dried in vacuum at 150 °C for 8 h before use for better solubility in electrolyte solvents [47].

Cathodes were cast on an Al-foil from a slurry using variable spreading gaps (100 and 250 μm). The slurries were made using a mixture of CF_x , binder and carbon black at a mass ratio of 8:1:1, respectively, unless otherwise noted. The CF_x was ultrasonicated for 4 hours in ethanol (EtOH) following similar ultrasonication processes of the literature [48,49] for exfoliation and easier homogenization of the slurry. A Branson Ultrasonics CPX952516R device was used that allows for mild ultrasonication (40 kHz). The binders were added in the form of a 4 w% PAN/DMF or PVDF/NMP solution to the dry solid CF_x and CB and mixed thoroughly in a laboratory mixer (Thinky ARM-310). The cathodes were dried in a vacuum oven at 120 °C for 8h. A more detailed account on our laboratory procedures is available in Ref [50].

The $LiOX \cdot BF_3$ additive [51] was synthesized in the presence of CF_x by mixing CF_x with Li_2CO_3 in a 20:1 molar ratio and ultrasonating the mixture in $F_3B \cdot OEt_2$ for 4 h. The product was washed with dichloromethane and filtered on a nanoporous filter. Products were dried in vacuum after ultrasonication.

Cathode disks of 0.65 cm radius were punched out of the cathode sheets and placed into CR2032 coin cell cases. Porous polypropylene disks (Celgard 2500, 25 μm thickness) were used as separator and Li-foil disks as anodes. For electrolyte, a 1 M solution of $LiBF_4$, $LiClO_4$, $LiPF_6$ or LiBOB was used in a 1:1:1 volumetric mixture of PC, DME and DOL solvents following a similar electrolyte in Ref [52]. The advantages of using DOL as an electrolyte (co)solvent are discussed in Ref [53]. Typically, a 60 μL electrolyte was filled in a coin cell. The cells were hermetically sealed using a crimping machine.

Galvanostatic cycling of coin cell batteries was carried out using a Neware battery tester (maximum voltage 5V, maximum current 50 mA). The voltage limits were 1.5 and 4.6 V, unless otherwise noted. Electrochemical Impedance Spectra (EIS) were measured using a PARSTAT 4000 instrument between 0.1 Hz and 100 kHz at a 10 mV amplitude. XRD was carried out using a Bruker D2 Phaser device at Cu $K\alpha$ X-ray radiation (1.5406 Å wavelength). Additionally, synchrotron XRD (at 0.459063 Å wavelength) was also carried out at the Advanced Photon Source at Argonne National Laboratory.

3. Results and Discussion

We tested a series of Li-CF_x cells to understand the binder and electrolyte dependence of the power density. The compositions of these cells are listed in Table 1.

Table 1. Cathode composition in different groups of cells. Blends of solvents were obtained by mixing equal volumetric amounts of the components. CF_x was ultrasonicated for 4 h before use except in the case of H304 (0 h) and H101 (3 h). The active material loading was 1.0-1.5 mg/cm² for 100 μm thick cathodes and 3.0-4.6 mg/cm² for 250 μm ones. The concentration of the electrolytes was always 1 M. The molar ratio of CF_x to the LiOX·BF₃ additive (when present) was 10:1.

Group ID	Ultrasonication of CF _x		Thickness (μm)	Binder	Electrolyte	
	Solvent	Additive			Salt	Solvent
H293	EtOH	-	100	PAN	LiBF ₄	PC:DME:DOL
H314	EtOH	-	250	PAN	LiBF ₄	PC:DME:DOL
H214	EtOH	-	100	PVDF	LiBF ₄	PC:DME:DOL
H321	EtOH	-	250	PVDF	LiBF ₄	PC:DME:DOL
H366	EtOH	-	100	PAN	LiPF ₆	PC:DME:DOL
H371	EtOH	-	100	PAN	LiClO ₄	PC:DME:DOL
H429	EtOH	-	100	PAN	LiBOB	PC:DME:DOL
H101	F ₃ B·OEt ₂	-	100	PVDF	LiBF ₄	PC:DME:DOL
H274	F ₃ B·OEt ₂	LiOX·BF ₃	100	PAN	LiBF ₄	PC:DME:DOL
H304	no ultrasonication		100	PAN	LiBF ₄	PC:DME:DOL
H179	F ₃ B·OEt ₂	LiOX·BF ₃	100	PAN	LiBF ₄	DMSO:DOL
H387	EtOH	-	100	PVDF	LiBF ₄	EC:DMC

The composition of the cells in Table 1 reflects the time evolution of our research toward increasingly high power Li-CF_x batteries and toward understanding the key factors that control power density. The higher the number in the cell group ID the later the composition was explored.

The gravimetric energy vs power density curves of cells with 100 μm thick cathodes and 1M LiBF₄ electrolytes are shown in Fig 2. The values are given with respect to the weight of the CF_x in the cathode. These cells differ in the type of the binder (PAN or PVDF) and the preparation of the CF_x active material (ultrasonication duration, solvent and additive). The C rates of the discharge were between 0.05 and 40.

For a reference Li-CF_x cell of traditional composition, we choose the same cell composition as the one in Ref [37] that investigated the effects of a gaseous BF₃ electrolyte additive. It uses a PVDF binder and a 1 M LiBF₄ electrolyte in EC:DMC(1:1). This configuration (group H387) is highly inferior in performance to all but one of the cell configurations investigated here.

The best performing cells are from group H293. These cells provide the highest energy density at very high power density and perform consistently better than other cells at higher than 10 kW/kg power density. Group H293 cells have a simple composition: their cathodes are composed of CF_x that was ultrasonicated in EtOH for 4 h and the binder was PAN, no additive or special solvent (such as F₃B·OEt₂) was applied.

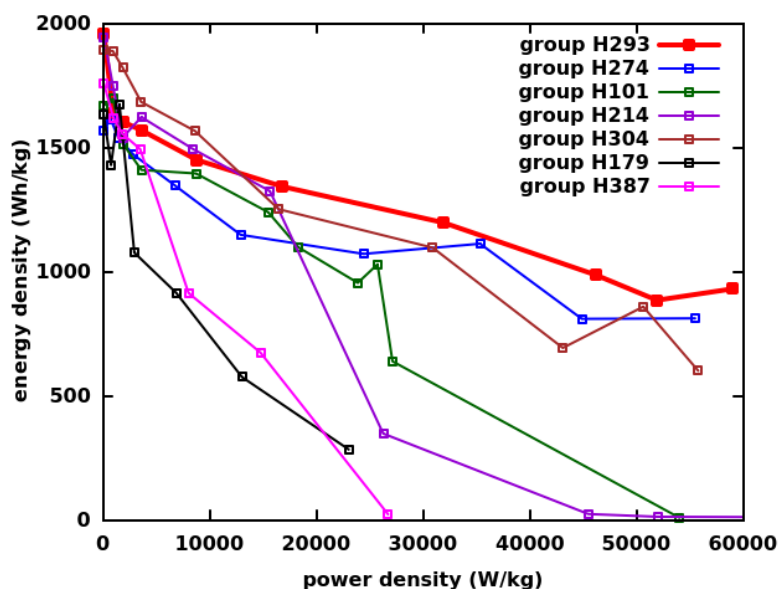


Figure 2. Gravimetric energy density vs power density of cells containing cathodes with $100\ \mu\text{m}$ layer thickness. Each cell contained a 1M LiBF_4 electrolyte. The binder was either PAN or PVDF. The detailed composition of the cells can be found in Table 1.

The voltage vs capacity density curves during the discharge of group H293 cells can be seen in Fig 3. They compare very well (especially for high C rates) with similar curves in the best performing CF_x cells of the literature, such as those in Refs [33–37] and especially those in Ref [32] which we consider the probably best performing CF_x cell demonstrated to date. While the CF_x used in Ref [32] is based on fluorinated graphene microspheres, our method uses the traditional and much easier to synthesize graphite fluoride. Other components of our cathode, such as the PAN binder and the electrolyte (1M LiBF_4 in PC:DME:DOL(1:1:1)), are also conveniently available. Therefore, our method appears to offer a more economic composition and implementational simplicity while providing a competitive performance.

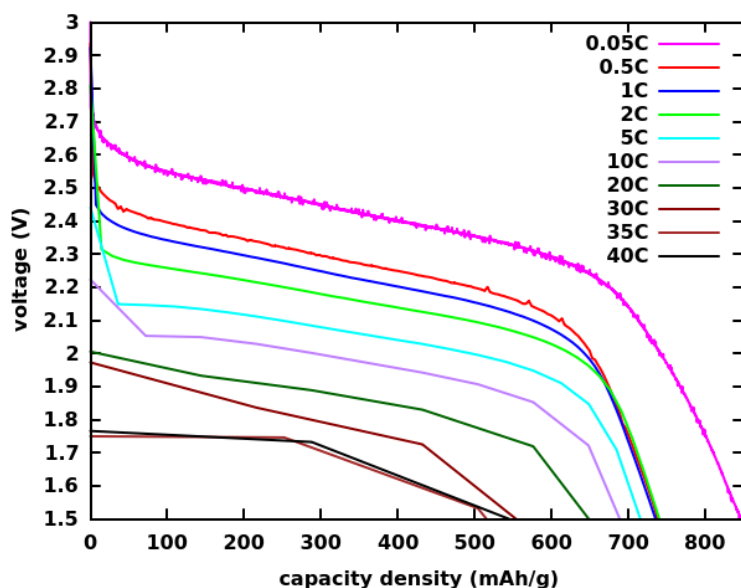


Figure 3. Voltage vs capacity density curves at various C rates for CF_x batteries in our best performing cells that provide the highest energy density at very high power densities (group H293).

Surprisingly, even the as purchased CF_x (with no ultrasonication, group H304) allows for relatively high energy densities at high power densities when used with a PAN binder and LiBF_4 electrolyte. However, when the PAN binder is exchanged to PVDF, the the energy density rapidly decays at high power densities (group H214). If the CF_x is ultrasonicated in $\text{F}_3\text{B}\cdot\text{OEt}_2$ then the performance becomes better even if PVDF binder is used (group H101), however, it is still much inferior to group H293. This indicates the beneficial effects of BF_3 on the power density similarly to Ref [37]. The ultrasonication of CF_x in $\text{F}_3\text{B}\cdot\text{OEt}_2$ with the $\text{LiOX}\cdot\text{OEt}_2$ additive (group H274) does not improve the performance of a simple ultrasonicated CF_x active material when PAN binder is used. This stresses again the robustness of the group H293 cathodes.

We have also explored a 1:1 volumetric mixture of DMSO and DOL as a solvent in a 1M LiBF_4 electrolyte as it was found in earlier literature that such an electrolyte can raise the discharge voltage [54] at slow discharge. In our experience, this electrolyte has a poor performance at high C rates (high power density) even when used with a PAN binder (group H179).

Next, we have investigated the effect of cathode thickness on the performance of Li- CF_x cells while using either PAN or PVDF binder and keeping the 1 M LiBF_4 electrolyte in PC:DME:DOL(1:1:1). Two different cathode thickness were used, 100 μm (1.0-1.5 mg/cm^2 CF_x loading) and 250 μm (3.0-4.6 mg/cm^2 CF_x loading). Cathodes with PAN binder have a greatly superior performance to cathodes with PVDF binder at higher power densities (over 10 kW/kg), independent from cathode thickness as shown in Fig 4.

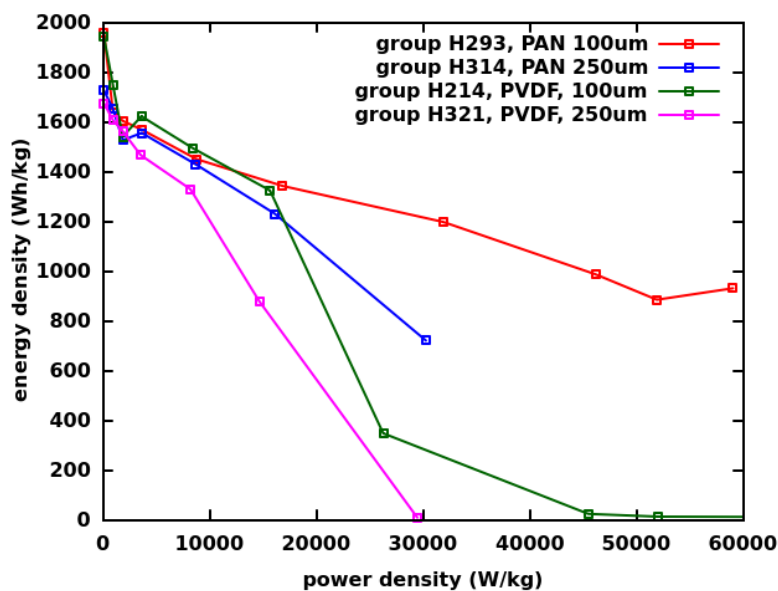


Figure 4. The dependence of the energy vs power density performance on the type of the binder (PAN or PVDF) and on the thickness of the cathode (100 or 250 μm). The electrolyte was 1 M LiBF_4 in PC:DME:DOL(1:1:1).

We have also explored how the choice of the electrolyte salt influences the performance of Li- CF_x cells with PAN binder. 1 M solutions of LiBF_4 , LiClO_4 , LiPF_6 and LiBOB were used in PC:DME:DOL(1:1:1). Fig 5 shows the dependence of the energy vs power density performance on the type of the electrolyte. There is a divergent performance at greater than 5 kW/kg power density: LiBF_4 performs best, followed relatively closely by LiClO_4 while LiPF_6 performs much less well and LiBOB is by far the slowest discharging one.

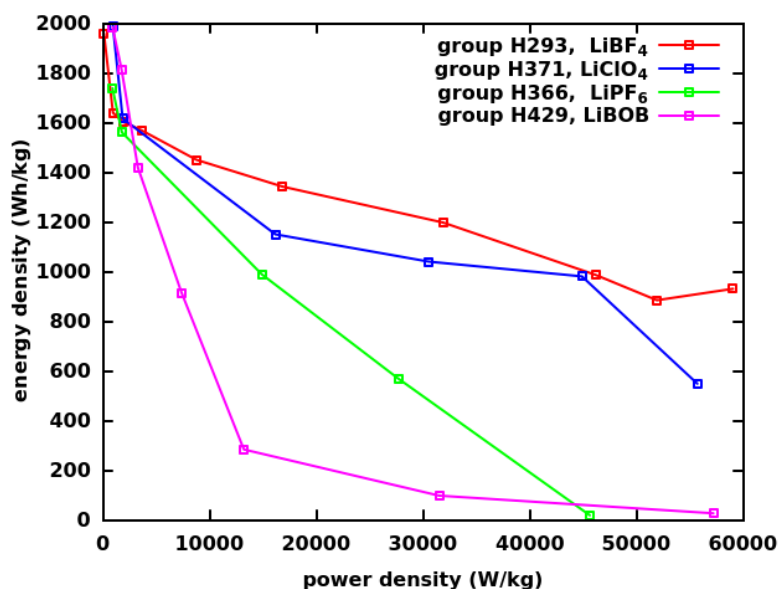


Figure 5. The dependence of the energy vs power density performance on the type of the electrolyte. The effects of LiBF₄, LiClO₄, LiPF₆ and LiBOB electrolyte salts in PC:DME:DOL(1:1:1) solvent are investigated. The cathode thickness was approximately 100 μm in all cases.

Figure 6 shows the impedances (Z) of the electrolytes before (panel **a**) and 1 h after (panel **b**) full discharge at 0.5 C rate. The higher frequency impedances are close to the origin while the low frequency ones are farther away. The slope of the near straight section is proportional to the diffusion coefficient of Li⁺ ions and the steeper the slope the higher the ionic conductivity of the electrolyte. The maximum extent of the semicircle (formed after discharge) on the Re(Z) axis is related to the charge transfer resistance in the system: the smaller the semi-circle the faster the charge transfer and the higher the power density. The intercept of the impedance curve with the Re(Z) axis is the bulk resistivity in the system (not discussed here). The charge transfer is fastest in the LiBF₄ and LiClO₄ electrolytes while it is much slower in the LiPF₆ and LiBOB electrolytes. These observations are in agreement with the measured power densities discussed above.

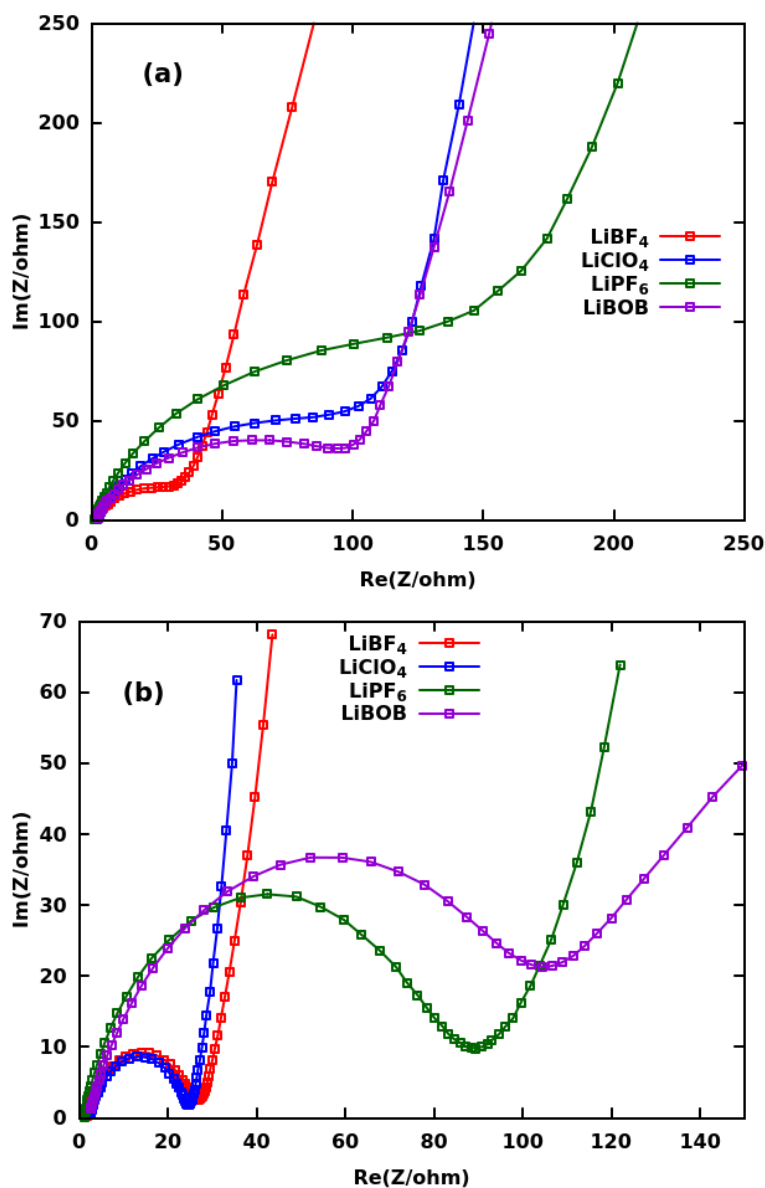


Figure 6. Impedance (Z) of Li-CF_x cells with 1 M LiBF₄, LiClO₄, LiPF₆ and LiBOB electrolytes before (panel a) and 1 h after (panel b) full discharge at 0.5 C rate. The electrolyte solvent was PC:DME:DOL(1:1:1).

Synchrotron XRD measurements were carried out on the discharged Li-CF_x cells with PAN and PVDF binders in order to investigate the extent of the hypothetical inhibition of LiF crystallization by the PAN binder. The cells were discharged at 0.5 C rate using 250 μm thick cathodes. We found a large amount of crystalline LiF discharge product, as indicated in Fig 7. The broad peaks at 5.9-7.4 and 10-15 degrees region indicate the presence of intercalated graphite and turbostratic graphite like structures, respectively. Our experience is contradictory to that of Ref [37] which found no crystalline LiF in the XRD patterns of the discharged CF_x cathodes when a small concentration of BF₃ gas in the electrolyte was used. Therefore, we cannot confirm a similar degree of inhibition of LiF formation when the PAN binder is used. It is however possible that the inhibition caused by the PAN binder only slows down the LiF formation on a shorter time scale during discharge and therefore it could not be detected by our synchrotron XRD measurements about three weeks after the discharge. Consequently, the inhibition mechanism proposed by Jones and Hossain in Ref [39] may still be valid.

Also note that Jones and Hossain did not mention any electrolyte effects on their proposed inhibition mechanism of the LiF crystallization. Our study points out the first time in the literature that a combined effect of the binder and the electrolyte can be a simple and robust means of greatly increasing the power density of Li- CF_x cells.

Further analysis of the XRD of the discharge products also suggests that it may contain both turbostratic graphite (the broad peak at 7.4 degrees near the (002) reflection of graphite) and a first stage intercalation complex of graphite (the broad peak at 5.9 degrees). Unfortunately, we could not further investigate if these broad peaks might be associated with hard carbon as suggested in Ref [29].

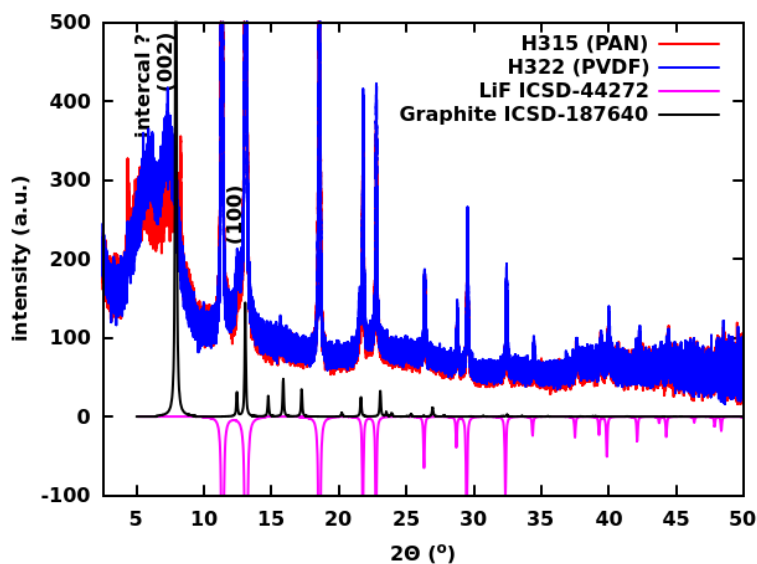


Figure 7. Synchrotron XRD patterns of the discharged cathodes of Li- CF_x cells with PAN and PVDF binders as compared to the patterns of graphite and LiF. The intensities of the LiF pattern are represented on the negative scale for clarity. The approximate locations of the graphite (002) and (100) reflections above the broad peaks are also indicated. These broad peaks are associated with turbostratic graphite and intercalated graphite.

As the improvement of the power density is a combined effect of the binder and the electrolyte, the understanding of the interaction of PAN with various electrolytes attracts our attention. It has been known for a few decades that solid polymer electrolytes can be made from PAN and LiClO_4 solution in some organic solvents [55,56]. The ionic conductivity of these electrolytes depend on the ratio of their components and can be as high as 10^{-3} - 10^{-2} S/cm [56]. Potentially, the presence of such a polymer electrolyte in our CF_x cathodes may contribute to the enhanced discharge power density.

The mechanistic origin of the observed combined binder and electrolyte effects on the power density is not clear yet. Several analogous reactions however point toward the electro-catalytic effect of PAN in the given circumstances. As PAN $((\text{CH}_2\text{CH}-\text{CN})_x)$ has cyano (-CN) group side chains, it is reasonable to assume that these -CN groups would be oxidized by CF_x in a similar manner to the oxidation of NaCN by CF_x [57]:



The resulting $\cdot\text{CN}$ radicals mostly dimerize to cyanogen (NC-CN) and then polymerize to paracyanogen $(\text{CN})_{2n}$ [57] and to a smaller extent may covalently functionalize the graphene sheets [58]. In PAN, an oxidative effect by CF_x is expected to result in the polymerization of the -CN groups in the side chain. Such a side chain polymerization of PAN has been known for long as an effect of heating and it results in pyridine type rings and a ladder type polymer [59].

We propose that the side chain polymerized PAN (PPAN) functions as an electro-catalyst. The catalytic mechanism is depicted in Fig 8. PPAN and CF_x form a cyclo-adduct after the nucleophilic attack of PPAN on CF_x . This cyclo-adduct is the activated complex of the reaction mechanism. When the battery discharges, the cyclo-adduct is reduced

and splits into a residual CF_x with a newly formed $\text{C}=\text{C}$ double bond and a recycled PPAN, while also LiF is formed. The catalytic cycle can be active as long as there is a supply of Li and C-F bonds. It seems, that PPAN must move on the surface of CF_x in order to harvest new C-F bonds. This motion of PPAN can be beneficial for opening up the space between stacked CF_x layers. This may be the reason that the catalytic effect works quite well even on non-ultrasonicated CF_x . It is further expected that some electrolyte anions, such as PF_6^- and BOB^- may irreversibly react with PAN or PPAN and poison the catalyst. PF_6^- may form P-N bonds with PPAN while the $\text{C}=\text{O}$ double bonds in BOB^- may form cyclo-adducts with PAN. Other electrolytes, such as BF_4^- and ClO_4^- do not react irreversibly with PPAN and thus they do not poison the catalyst. Further note that the pyridine-like units in PPAN are also reminiscent of the pyridine derivative 4-Dimethylaminopyridine (DMAP) which was successfully applied as a catalyst in the reaction of NaOH and CF_x and yielded $-\text{OH}$ functionalized graphene (and presumably also HO-OH , analogously to NC-CN of Eq 2) [60]. As PVDF and PTFE binders are not reactive with CF_x , they cannot provide catalytic effects. Therefore, the proposed catalytic mechanism can account for all the observed phenomena.

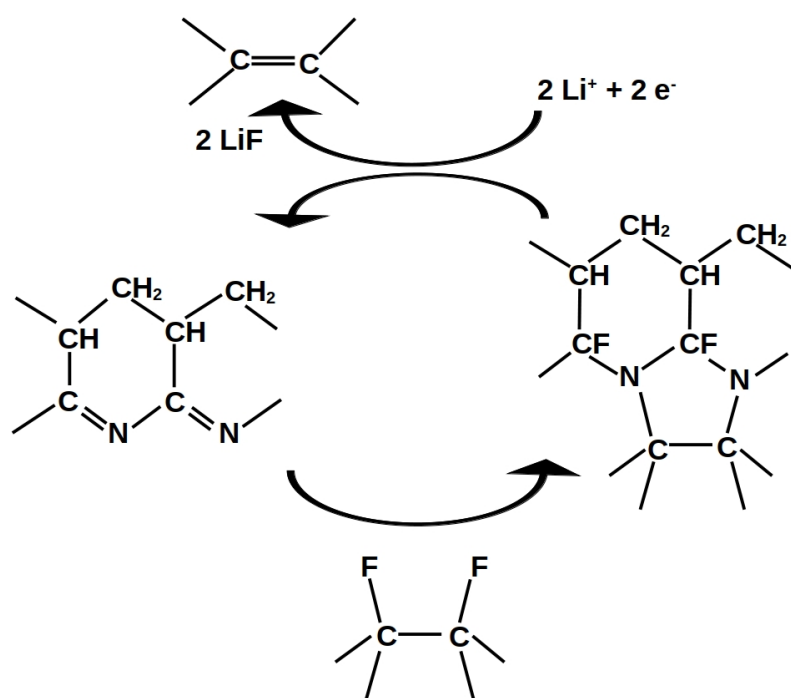


Figure 8. The proposed electro-catalytic action of the PAN binder on CF_x during the discharge of the Li-CF_x cell. PAN is represented in its side-chain polymerized form (PPAN), two repeating units are shown with $\text{C}=\text{N}$ double bonds. The N atoms of the PAN commit a nucleophilic attack on the C atoms of CF_x . In the resulting activated complex, PAN is bound to the CF_x surface via C-N bonds while the F atoms migrate to PAN and form new C-F bonds on PAN. The formation of the activated complex is a cycloaddition involving $\text{C}=\text{N}$ double bonds. When the battery discharges, LiF forms, while the activated complex splits into a residual CF_x with a newly formed $\text{C}=\text{C}$ double bond and the original PAN is recycled. The cycle can be repeated as long as there is sufficient Li and C-F supply.

4. Conclusions

In the present study, we have demonstrated that the choice of the binder and electrolyte plays a crucial role in achieving very high power densities in Li-CF_x batteries. As high as 931 Wh/kg energy density could be achieved at 59 kW/kg power density in a coin cell when a PAN binder and LiBF_4 electrolyte are used. While a former theoretical proposal by Jones and Hossain predicted tremendous binder effects on the performance of Li-CF_x cells [39] assuming that certain binders will inhibit the crystallization of the discharge product LiF , their proposal was not aware of the role of the electrolyte in such effects. The origin of the combined binder and electrolyte effect is not clear yet. Based on the analogy to the proven oxidation of NaCN by CF_x , we propose that PAN plays the role of an electro-catalyst in the

discharge of CF_x as long as an electrolyte is available that is able to reversibly bind to PAN. Our method represents a simple and efficient route to very high power primary Li- CF_x batteries.

Author Contributions: Conceptualization and experiment planning: K.N.; experimental work: H.H and K.N.; analysis, K.N., H.H. and L.S.; original draft preparation and proposed electro-catalytic mechanism: K.N.; review and editing: K.N., H.H. and L.S.

Funding: This research was funded in most part by the U.S. National Science Foundation under a STTR Phase I grant to Boron Nitride Power LLC and IIT (award number 2109286). Additional private funding was provided by Boron Nitride Power LLC.

Data Availability Statement: Data generated in the present work is available upon request from the authors.

Acknowledgments: This research used resources (particularly synchrotron XRD facilities) of the Advanced Photon Source, a U.S. Department of Energy (DOE) Office of Science user facility operated for the DOE Office of Science by Argonne National Laboratory under Contract No. DE-AC02-06CH11357.

Conflicts of Interest: The authors declare no conflict of interest. The funders had no role in the design of the study; in the collection, analyses, or interpretation of data; in the writing of the manuscript, or in the decision to publish the results.

References

1. Trahey, L.; Brushett, F.R.; Balsara, N.P.; Ceder, G.; Cheng, L.; Chiang, Y.M.; Hahn, N.T.; Ingram, B.J.; Minter, S.D.; Moore, J.S.; et al. Energy storage emerging: A perspective from the Joint Center for Energy Storage Research. *Proceedings of the National Academy of Sciences* **2020**, *117*, 12550–12557.
2. Yang, X.G.; Liu, T.; Ge, S.; Rountree, E.; Wang, C.Y. Challenges and key requirements of batteries for electric vertical takeoff and landing aircraft. *Joule* **2021**, *5*, 1644–1659.
3. Bills, A.; Sripad, S.; Fredericks, W.L.; Singh, M.; Viswanathan, V. Performance metrics required of next-generation batteries to electrify commercial aircraft. *ACS Energy Letters* **2020**, *5*, 663–668.
4. Krause, F.; Ruiz, J.; Jones, S.; Brandon, E.; Darcy, E.; Iannello, C.; Bugga, R. Performance of commercial Li-ion cells for future NASA missions and aerospace applications. *Journal of The Electrochemical Society* **2021**, *168*, 040504.
5. Krause, F.C.; Jones, J.P.; Jones, S.C.; Pasalic, J.; Billings, K.J.; West, W.C.; Smart, M.C.; Bugga, R.V.; Brandon, E.J.; Destephen, M. High specific energy lithium primary batteries as power sources for deep space exploration. *Journal of the Electrochemical Society* **2018**, *165*, A2312.
6. Ndzebet, E.; Destephen, M.; Zhang, D.; Darch, D. High Power and High Rate Li/CF_x-MnO₂ Pouch Cell Hybrid Technology. In Proceedings of the 48th Power Sources Conference; , 2018; pp. 558–561.
7. Greatbatch, W.; Holmes, C.; Takeuchi, E.; Ebel, S. Lithium/carbon monofluoride (Li/CF_x): a new pacemaker battery. *Pacing and clinical electrophysiology* **1996**, *19*, 1836–1840.
8. Ruff, O.; Bretschneider, O. Die Reaktionsprodukte der verschiedenen Kohlenstoffformen mit Fluor II (Kohlenstoff-monofluorid). *Zeitschrift für anorganische und allgemeine Chemie* **1934**, *217*, 1–18.
9. Rüdorff, W.; Rüdorff, G. Zur Konstitution des Kohlenstoff-Monofluorids. *Zeitschrift für anorganische Chemie* **1947**, *253*, 281–296.
10. Watanabe, N.; Fukuda, M. Primary cell for electric batteries. *US Patent 3536532* **1970**.
11. Watanabe, K.; Fukuda, M. High energy density battery. *US Patent 3700502* **1972**.
12. Fukuda, M.; Iijima, T.; Toyoguchi, Y. Active material for positive electrode of battery. *US Patent 4271242* **1981**.
13. Sharma, N.; Dubois, M.; Guérin, K.; Pischedda, V.; Radescu, S. Fluorinated (Nano) Carbons: CF_x Electrodes and CF_x-Based Batteries. *Energy Technology* **2021**, *9*, 2000605.
14. Ahmad, Y.; Batisse, N.; Chen, X.; Dubois, M. Preparation and Applications of Fluorinated Graphenes. *C* **2021**, *7*, 20.
15. Wang, D.; Wang, G.; Zhang, M.; Cui, Y.; Yu, J.; Shi, S. Composite cathode materials for next-generation lithium fluorinated carbon primary batteries. *Journal of Power Sources* **2022**, *541*, 231716.
16. Groult, H.; Tressaud, A. Use of inorganic fluorinated materials in lithium batteries and in energy conversion systems. *Chemical Communications* **2018**, *54*, 11375–11382.
17. Zhang, Q.; Takeuchi, K.J.; Takeuchi, E.S.; Marschilok, A.C. Progress towards high-power Li/CF_x batteries: electrode architectures using carbon nanotubes with CF_x. *Physical Chemistry Chemical Physics* **2015**, *17*, 22504–22518.
18. Chen, P.; Jiang, C.; Jiang, J.; Zou, J.; Ran, Q.; Wang, X.; Niu, X.; Wang, L. Fluorinated Carbons as Rechargeable Li-Ion Battery Cathodes in the Voltage Window of 0.5–4.8 V. *ACS Applied Materials & Interfaces* **2021**, *13*, 30576–30582.
19. Liu, W.; Li, H.; Xie, J.Y.; Fu, Z.W. Rechargeable room-temperature CF_x-sodium battery. *ACS Applied Materials & Interfaces* **2014**, *6*, 2209–2212.
20. Whittingham, M.S. Mechanism of reduction of the fluorographite cathode. *Journal of The Electrochemical Society* **1975**, *122*, 526.

21. Watanabe, N.; Nakajima, T.; Hagiwara, R. Discharge reaction and overpotential of the graphite fluoride cathode in a nonaqueous lithium cell. *Journal of Power Sources* **1987**, *20*, 87–92.
22. Watanabe, N.; Hagiwara, R.; Nakajima, T.; Touhara, H.; Ueno, K. Solvents effects on electrochemical characteristics of graphite fluoride—lithium batteries. *Electrochimica Acta* **1982**, *27*, 1615–1619.
23. Jang, B.Z.; Liu, C.; Neff, D.; Yu, Z.; Wang, M.C.; Xiong, W.; Zhamu, A. Graphene surface-enabled lithium ion-exchanging cells: next-generation high-power energy storage devices. *Nano Letters* **2011**, *11*, 3785–3791.
24. Liu, C.; Zhamu, A.; Neff, D.; Jang, B.Z. Lithium super-battery with a functionalized nano graphene cathode, 2014. US Patent 8,795,899.
25. Kim, H.; Park, K.Y.; Hong, J.; Kang, K. All-graphene-battery: bridging the gap between supercapacitors and lithium ion batteries. *Scientific reports* **2014**, *4*, 5278.
26. Kim, H.; Park, Y.U.; Park, K.Y.; Lim, H.D.; Hong, J.; Kang, K. Novel transition-metal-free cathode for high energy and power sodium rechargeable batteries. *Nano Energy* **2014**, *4*, 97–104.
27. Kornilov, D.; Penki, T.R.; Cheglakov, A.; Aurbach, D. Li/graphene oxide primary battery system and mechanism. *Battery Energy* **2022**, *1*, 20210002.
28. Zhang, S.S.; Foster, D.; Wolfenstine, J.; Read, J. Electrochemical characteristic and discharge mechanism of a primary Li/CFx cell. *Journal of Power Sources* **2009**, *187*, 233–237.
29. Sayahpour, B.; Hirsh, H.; Bai, S.; Schorr, N.B.; Lambert, T.N.; Mayer, M.; Bao, W.; Cheng, D.; Zhang, M.; Leung, K.; et al. Revisiting discharge mechanism of CFx as a high energy density cathode material for lithium primary battery. *Advanced Energy Materials* **2022**, *12*, 2103196.
30. Yazami, R.; Hamwi, A.; Guérin, K.; Ozawa, Y.; Dubois, M.; Giraudet, J.; Masin, F. Fluorinated carbon nanofibres for high energy and high power densities primary lithium batteries. *Electrochemistry communications* **2007**, *9*, 1850–1855.
31. Lam, P.; Yazami, R. Physical characteristics and rate performance of (CFx)_n (0.33 < x < 0.66) in lithium batteries. *Journal of Power Sources* **2006**, *153*, 354–359.
32. Luo, Z.; Wang, X.; Chen, D.; Chang, Q.; Xie, S.; Ma, Z.; Lei, W.; Pan, J.; Pan, Y.; Huang, J. Ultrafast Li/fluorinated graphene primary batteries with high energy density and power density. *ACS Applied Materials & Interfaces* **2021**, *13*, 18809–18820.
33. Dai, Y.; Cai, S.; Wu, L.; Yang, W.; Xie, J.; Wen, W.; Zheng, J.C.; Zhu, Y. Surface modified CFx cathode material for ultrafast discharge and high energy density. *Journal of Materials Chemistry A* **2014**, *2*, 20896–20901.
34. Peng, C.; Kong, L.; Li, Y.; Fu, H.; Sun, L.; Feng, Y.; Feng, W. Fluorinated graphene nanoribbons from unzipped single-walled carbon nanotubes for ultrahigh energy density lithium-fluorinated carbon batteries. *Science China Materials* **2021**, *64*, 1367–1377.
35. Jiang, S.; Huang, P.; Lu, J.; Liu, Z. The electrochemical performance of fluorinated ketjenblack as a cathode for lithium/fluorinated carbon batteries. *RSC advances* **2021**, *11*, 25461–25470.
36. Wang, K.; Feng, Y.; Kong, L.; Peng, C.; Hu, Y.; Li, W.; Li, Y.; Feng, W. The fluorination of boron-doped graphene for CFx cathode with ultrahigh energy density. *Energy & Environmental Materials*, p. e12437.
37. Li, Q.; Xue, W.; Sun, X.; Yu, X.; Li, H.; Chen, L. Gaseous electrolyte additive BF₃ for high-power Li/CFx primary batteries. *Energy Storage Materials* **2021**, *38*, 482–488.
38. Rangasamy, E.; Li, J.; Sahu, G.; Dudney, N.; Liang, C. Pushing the theoretical limit of Li-CF_x batteries: a tale of bifunctional electrolyte. *Journal of the American Chemical Society* **2014**, *136*, 6874–6877.
39. Jones, S.C.; Hossain, S. Polymer materials as binder for a CFx cathode, 2011. US Patent App. 13/010,431.
40. Németh, K. Materials design by quantum-chemical and other theoretical/computational means: Applications to energy storage and photoemissive materials. *International Journal of Quantum Chemistry* **2014**, *114*, 1031–1035.
41. Zhang, F.; Németh, K.; Bareño, J.; Dogan, F.; Bloom, I.D.; Shaw, L.L. Experimental and theoretical investigations of functionalized boron nitride as electrode materials for Li-ion batteries. *RSC Advances* **2016**, *6*, 27901–27914.
42. Németh, K. Simultaneous oxygen and boron trifluoride functionalization of hexagonal boron nitride: a designer cathode material for energy storage. *Theoretical Chemistry Accounts* **2018**, *137*, 157.
43. Németh, K. Radical anion functionalization of two-dimensional materials as a means of engineering simultaneously high electronic and ionic conductivity solids. *Nanotechnology* **2021**, *32*, 245709.
44. Németh, K. Functionalized boron nitride materials as electroactive species in electrochemical energy storage devices. *US Patent 10,693,137* **2020**.
45. Németh, K. Radical Anion Functionalization of Two-dimensional Materials. *US Patent 11,453,596 B2* **2022**.
46. Marshall, J.E.; Zhenova, A.; Roberts, S.; Petchey, T.; Zhu, P.; Dancer, C.E.; McElroy, C.R.; Kendrick, E.; Goodship, V. On the solubility and stability of polyvinylidene fluoride. *Polymers* **2021**, *13*, 1354.
47. Zor, C.; Subaşı, Y.; Hacıu, D.; Somer, M.; Afyon, S. Guide to water free lithium bis (oxalate) borate (LiBOB). *The Journal of Physical Chemistry C* **2021**, *125*, 11310–11317.

48. Zhang, M.; Ma, Y.; Zhu, Y.; Che, J.; Xiao, Y. Two-dimensional transparent hydrophobic coating based on liquid-phase exfoliated graphene fluoride. *Carbon* **2013**, *63*, 149–156.
49. Zeng, X.; Peng, Y.; Yu, M.; Lang, H.; Cao, X.; Zou, K. Dynamic sliding enhancement on the friction and adhesion of graphene, graphene oxide, and fluorinated graphene. *ACS applied materials & interfaces* **2018**, *10*, 8214–8224.
50. Huo, H. High Energy High Power Primary Lithium Batteries with Graphite Fluoride and Functionalized Boron Nitride Cathodes. Master's thesis, Illinois Institute of Technology, 2022.
51. Tatagari, V.R. A Functionalized 2D Boron Nitride Electrode for Rechargeable Batteries. Master's thesis, Illinois Institute of Technology, 2021.
52. Li, Y.Y.; Liu, C.; Chen, L.; Wu, X.Z.; Zhou, P.F.; Shen, X.Y.; Zhou, J. Multi-layered fluorinated graphene cathode materials for lithium and sodium primary batteries. *Rare Metals* **2022**, pp. 1–14.
53. Zhao, Q.; Liu, X.; Zheng, J.; Deng, Y.; Warren, A.; Zhang, Q.; Archer, L. Designing electrolytes with polymerlike glass-forming properties and fast ion transport at low temperatures. *Proceedings of the National Academy of Sciences* **2020**, *117*, 26053–26060.
54. Pang, C.; Ding, F.; Sun, W.; Liu, J.; Hao, M.; Wang, Y.; Liu, X.; Xu, Q. A novel dimethyl sulfoxide/1, 3-dioxolane based electrolyte for lithium/carbon fluorides batteries with a high discharge voltage plateau. *Electrochimica Acta* **2015**, *174*, 230–237.
55. Watanabe, M.; Kanba, M.; Nagaoka, K.; Shinohara, I. Ionic conductivity of hybrid films composed of polyacrylonitrile, ethylene carbonate, and LiClO₄. *Journal of Polymer Science: Polymer Physics Edition* **1983**, *21*, 939–948.
56. Chen, H.; Lin, F.; Chen, C. Polyacrylonitrile electrolytes 1. A novel high-conductivity composite polymer electrolyte based on PAN, LiClO₄ and α -Al₂O₃. *Solid State Ionics* **2002**, *150*, 327–335.
57. Siedle, A.; Losovyj, Y.; Stein, B.D.; Pink, M.; Werner-Zwanziger, U. Cyanographite. *The Journal of Physical Chemistry C* **2022**, *126*, 3001–3008.
58. Bakandritsos, A.; Pykal, M.; Błoński, P.; Jakubec, P.; Chronopoulos, D.D.; Poláková, K.; Georgakilas, V.; Čépe, K.; Tomanec, O.; Ranc, V.; et al. Cyanographene and graphene acid: emerging derivatives enabling high-yield and selective functionalization of graphene. *ACS nano* **2017**, *11*, 2982–2991.
59. Chung, T.C.; Schlesinger, Y.; Etemad, S.; Macdiarmid, A.; Heeger, A. Optical studies of pyrolyzed polyacrylonitrile. *Journal of Polymer Science: Polymer Physics Edition* **1984**, *22*, 1239–1246.
60. Bai, L.; Xu, Y.; Liu, A.; Dong, L.; Zhang, K.; Li, W.S.; Zhao, F.G. Unusual graphite fluoride hydrolysis toward unconventional graphene oxide for high-performance supercapacitors and Li-ion batteries. *Chemical Engineering Journal* **2022**, *434*, 134639.